ADVANCED ELECTRONIC MATERIALS
www.advelectronicmat.de

Humidity-Dependent Characteristics of Few-Layer MoS_2 Field Effect Transistors

Hui Yang, Sa Cai, Dongping Wu, and Xiaosheng Fang**

2D semiconductors, such as molybdenum disulfide (MoS_2), are emerging materials for field effect transistor (FET) channels in the field of nano-electronics. These atomically thin 2D films are particularly sensitive to moisture due to their large specific surface area, making them promising candidates for humidity sensing applications. Studies on MoS_2 FET humidity sensor have indicated that there are two key factors contributing to the performance of such devices: the number of MoS_2 layer and the gate bias. However, no existing work has revealed the exact relation between humidity and electrical properties for few-layer MoS_2 FETs. Here, the effect of humidity on the electrical transport properties for back-gated tri- and six-layer MoS_2 FETs is explored. The on-state current of the tri-layer MoS_2 FET is heavily dependent on the relative humidity while that of the six-layer MoS_2 FET remains nearly unchanged when relative humidity varies. Moreover, a linear relationship between the hysteresis and relative humidity is found in both tri-layer and six-layer MoS_2 FETs. These results advance the understanding of the dependence of electronic properties on relative humidity for few-layer MoS_2 FET.

1. Introduction

In the past few years, atomically thin 2D semiconductor materials with single- to few-layer thickness have been investigated for a wide range of applications.[1–10] Among 2D semiconductor materials, molybdenum disulfide (MoS_2) has been studied the most extensively and has garnered tremendous attention because of its relatively large bandgap, high carrier mobility, excellent chemical thermal stability, and high surface-to-volume ratio.[11–15] The considerable development of MoS_2 field effect transistors (FETs) enables potential applications in fields such as future electronics and chemical sensors.[16–18]

Some available reports suggest that few-layer MoS_2 FETs could outperform single-layer FETs because of the following reasons: i) few-layer MoS_2 has a smaller bandgap thus it can boost the current drive of FETs; ii) few-layer MoS_2 is less sensitive to ambience due to the smaller specific surface area; iii) few-layer MoS_2 is more immune to noise in air; iv) few-layer MoS_2 is more suitable for practical fabrication process to form large-area films.[19,20] Despite the above mentioned stability and feasibility, few-layer MoS_2 is highly sensitive to temperature and environmental gas, which seems to be limitations but actually offers new direction for the applications of few-layer MoS_2.[19,21–24] The effects of environmental gas on few-layer MoS_2 FET have been extensively studied in bottom gate configuration, paving the way for chemical sensors where changes of resistance and drain current are responsible for a successful detection.[23,24] Unfortunately, for these few-layer MoS_2 FETs, the humidity effects have not been systematically studied so far. Even though a few reports have discussed humidity-dependent transfer characteristics of MoS_2 FETs, these papers mainly focused on the single- or multilayer MoS_2 FETs.[25–28] Further, most of these works just demonstrated humidity sensing as proof-of-concept and failed to point out the subtleties of humidity-sensing performance and its relation to layered structures. To explore the intrinsic properties and improve the performance of few-layer MoS_2 FETs, thorough investigation of such humidity effects is required.

Herein, tri- and six-layer MoS_2 films were prepared to fabricate FET-based humidity sensors and their characteristics, including on-state current, mobility, subthreshold slop, and hysteresis, were measured and discussed. Specially, the transfer characteristics in the linear regime (at low drain voltage, V_{DS}) as a function of relative humidity (RH) in darkness were investigated to reveal the effect of humidity on the FETs. These results show that humidity significantly affects the electrical properties of few-layer MoS_2 FETs.

2. Results and Discussion

The architecture of the few-layer MoS_2 FETs was shown in **Figure 1**a, where exfoliated MoS_2 was transferred to the Si/SiO_2 substrate and Cr/Au electrodes were deposited. Roman spectrums of tri- and six-layer MoS_2 films were measured and E^1_{2g} and A_{1g} modes, whose frequency difference ($\Delta\lambda$) is conventionally used to predict the film thickness,[29–31] were observed as

Dr. H. Yang, S. Cai, Prof. X. S. Fang
Department of Materials Science
Fudan University
Shanghai 200433, China
E-mail: xshfang@fudan.edu.cn

Prof. D. P. Wu
State Key Laboratory of ASIC and System
Fudan University
Shanghai 200433, China
E-mail: dongpingwu@fudan.edu.cn

The ORCID identification number(s) for the author(s) of this article can be found under https://doi.org/10.1002/aelm.202000659.

DOI: 10.1002/aelm.202000659

ADVANCED ELECTRONIC MATERIALS
www.advelectronicmat.de

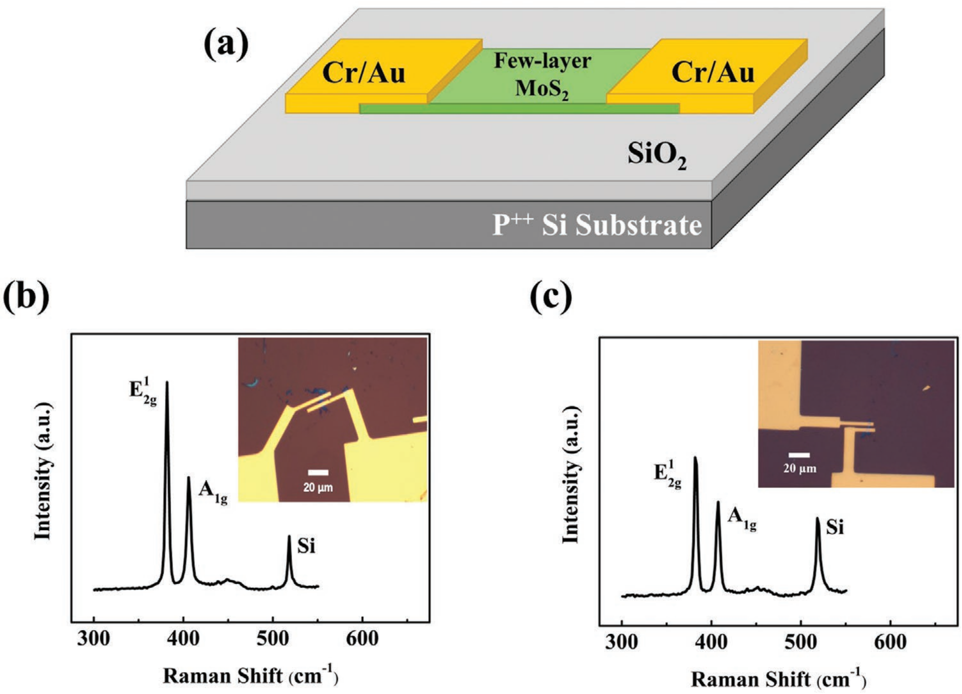

Figure 1. a) Schematic representation of few-layer MoS_2 FET with highly doped silicon as back gate, b) Raman spectrum of the tri-layer MoS_2 flake, inset is the corresponding optical image of the tri-layer MoS_2 FET, the channel length and width of the sample are $W = 4.6$ µm and $L = 3.0$ µm. c) Raman spectrum of the six-layer MoS_2 flake, inset is the corresponding optical image of the six-layer MoS_2 FET, the channel length and width of the sample are $W = 2.7$ µm and $L = 3.0$ µm. Scale bar: 20 µm.

shown in Figure 1b,c. The E^1_{2g} and A_{1g} peak position of these two MoS_2 films are summarized in Table S1, Supporting Information. Separations of 23.86 cm^{-1} and 25.12 cm^{-1} between peaks E^1_{2g} and A_{1g} were calculated from Raman spectrums, suggesting the number of layers of the MoS_2 films in Figure 1b,c to be 3 and 6, respectively. The weak bands at around 520 cm^{-1} is attributed to the mode of Si—Si vibration.[32]

Electrical properties of the tri-layer MoS_2 FET with channel length $L \approx 3.0$ µm and $W \approx 4.6$ µm (Figure 1b, inset) were subsequently characterized. **Figure 2**a shows the RH sensing current–voltage (I_{DS}–V_{BG}) behavior of the tri-layer MoS_2 FET, which exhibits conventional n-type behavior. With the RHs varying from 11.3% to 97.3%, the on-state currents (I_{ON}) show a strong modulation effect, changing from 63 to 179 nA at a 20 V back-gate voltage (V_{BG}), as shown in Figure 2b. The increase of I_{ON} with raising RH can be explained by the enhanced adsorption of water molecules on MoS_2 film. Once water molecules are introduced onto the MoS_2 channel, its electrons are transferred to the conduction band of MoS_2, leading to a conductivity increase of the MoS_2 FET.[33] The effect of gate bias on the RH-response of the tri-layer MoS_2 FET was also studied, as shown in Figure S1, Supporting Information. The results demonstrated that the I_{DS} of the tri-layer MoS_2 FET was more sensitive to RH when the positive gate bias was relatively low.

The dependence of the linear regime mobility (μ_{FE}) on the RH can be established by calculating it by the MOSFET square-law model,[34]

$$\mu_{FE} = \frac{dI_{DS}}{dV_{BG}} \frac{L}{WC_{OX}V_{DS}} \quad (1)$$

where C_{OX} is the oxide capacitance. And the Y-function method was hired to extract the intrinsic mobility (μ_0) excluding any contact resistance component,[35]

$$Y = I_{DS}/g_m^{1/2} = \left(\mu_0 C_{OX} W V_{DS}/L\right)^{1/2} \times (V_{BG} - V_{TH}) \quad (2)$$

where $g_m = dI_{DS}/dV_{BG}$ is the transconductance. V_{TH}, the threshold voltage, is extracted from the constant-current method at which the drain-source current is 1 nA. Figure 2c shows the positive correlation between μ_{FE}, μ_0, and RH, confirming the enhanced doping effect of adsorbed water molecules on MoS_2 surface with increased RHs, which is consistent with the above on-state current analysis. The negative correlation between the subthreshold slope (SS) and RH was revealed in Figure 2d, which was probably caused by the reduction of defects in tri-layer MoS_2 channel.[36] The detailed electrical characteristics including I_{ON}, μ_{FE}, μ_0, and SS of the tri-layer MoS_2 FET are listed in Table S2, Supporting Information.

Similar measurements were performed for the six-layer MoS_2 FET with channel length $L \approx 3.0$ µm and $W \approx 2.7$ µm (Figure 1c, inset) to compare its electronic properties with that of tri-layer MoS_2 FET. **Figure 3**a illustrates the I_{DS}–V_{BG} behavior of the six-layer MoS_2 FET under 11.3% to 97.3% RH, which shows the sample is also of n-type. In contrast with the strong responses to RH described in tri-layer MoS_2 FET, the dependence of the on-state current (I_{ON}) of six-layer MoS_2 FET on the RH was weak (<6%) and non-monotonic under 11.3% to 97.3% RH, as shown in Figure 3b. This weaker RH dependence of the I_{ON} could be explained by the smaller surface to volume ratio of the six-layer MoS_2 film compared to that of the tri-layer

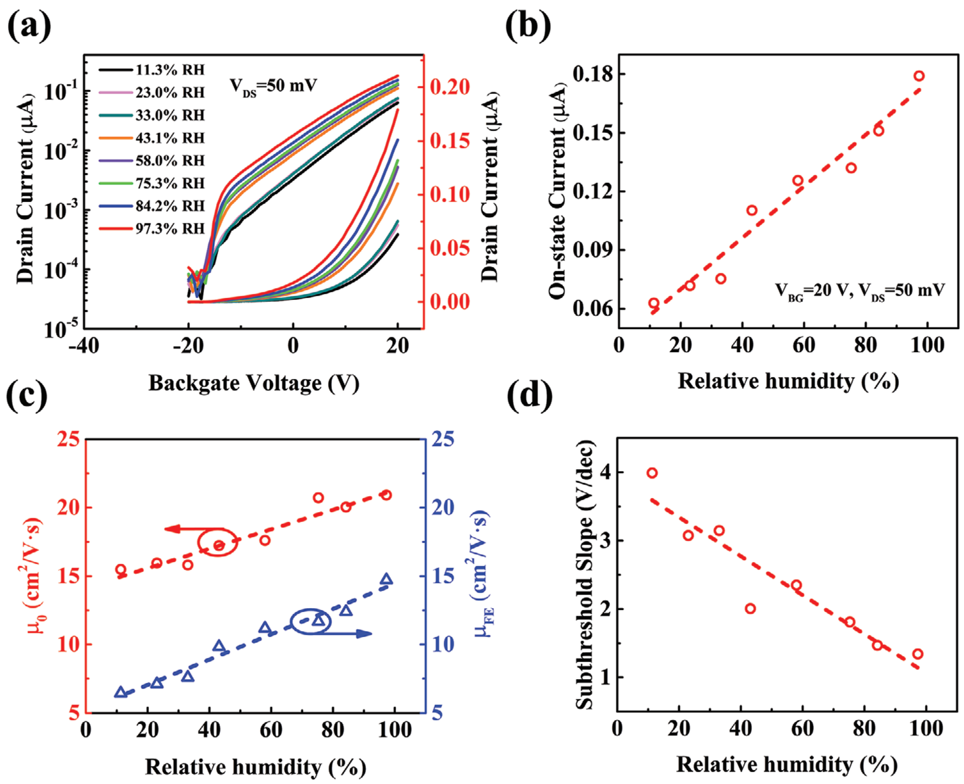

Figure 2. Electrical properties of the tri-layer MoS_2 FET device under different RHs. a) The transfer curves of the device with RHs increasing from 11.3% to 97.3% in both semi-logarithmic and linear scales (V_{DS} = 50 mV). b) The on-state current (I_{ON}) as functions of RH. c) The mobilities, including the field-effect mobility (μ_{FE}) and the intrinsic mobility (μ_0), as functions of RH. d) The subthreshold slope (SS) as functions of RH.

MoS_2 film.[20] We also studied the effects of positive gate bias on the RH-response of I_{DS} of the six-layer MoS_2 FET, shown in Figure S2, Supporting Information. The negative correlation between the sensitivity of I_{DS} to RH and positive gate bias was similar to the results shown in Figure S1, Supporting Information. However, the six-layer MoS_2 FET exhibited minor change in linear regime mobility (μ_{FE}) and intrinsic mobility (μ_0) when the RH varies from 11.3% to 97.3% (Figure 3c), which is slightly different from that of the tri-layer MoS_2 FET. More interesting, the positive correlation between SS and RH in six-layer MoS_2 FET (Figure 3d) exhibits a striking contrast with the negative correlation in tri-layer MoS_2 FET, which requires further investigations. Therefore, we conclude that only the electrical parameters in subthreshold region have been greatly affected by RH for the six-layer MoS_2 FET. The detailed electrical characteristics including I_{ON}, μ_{FE}, μ_0, and SS of the six-layer MoS_2 FET are listed in Table S3, Supporting Information.

Figure 4a shows the permeation process of water molecules in the six-layer and tri-layer MoS_2 films. As the number of layers increases, the penetration of water molecules between MoS_2 layers becomes more difficult. And most of adsorbed water molecules are concentrated on the surface of the MoS_2 film.[37] Figure 4b shows the schematic view of the current flow across the metal/MoS_2. When current flows across the junction, it encounters two resistances, the contact resistor $R_{contact}$ and sheet resistor R_{sheet} (Figure 4c).[38] R_{sheet1} and R_{sheet2} are the sheet resistors near the top and bottom of the MoS_2 film, respectively. Figure 4d shows the band diagrams of the few-layer MoS_2 FET. When the gate bias is 20 V (on-state), the energy levels of MoS_2 are pulled down and this leads to the thinning of the interfacial barrier and an increased tunneling probability of the carriers, resulting in low $R_{contact}$ and high I_{DS}. Also, R_{sheet2} is smaller than R_{sheet1} due to the high gate bias. Therefore, I_{DS} is mainly determined by R_{sheet2} rather than R_{sheet1}. As mentioned before, R_{sheet2} is less susceptible to RH when the number of layers increases. This explains why the I_{ON} of six-layer MoS_2 FET is less sensitive to RH than that of tri-layer MoS_2 FET. When the gate bias is low (off-state), the conduction band remains high and I_{DS} is dominated by thermionic emission current, resulting in high $R_{contact}$ and low I_{DS}. Therefore, I_{DS} is mainly determined by R_{sheet1} when the gate bias is low. Moreover, R_{sheet1} is more sensitive to RH than R_{sheet2}, which explains why the I_{DS} of MoS_2 FET has a higher RH-dependent sensitivity of I_{DS} at a lower positive gate bias.

Hysteresis, dominated by charging/discharging of oxide traps and affected by the defects on the channel, is typically observed in MoS_2 FETs.[39,40] Experimental findings suggest that the absorption of moisture on the oxide or channel surface will greatly affect the hysteresis of MoS_2 FETs exposed to the ambience.[25,41] **Figure 5**a presents the double sweep transfer curves of the tri-layer MoS_2 FET device. As expected, we observed a clockwise hysteresis related to RH, which is similar to what has been observed on single-[25] or multilayer[28] MoS_2-based FETs. Here, the magnitude of the hysteresis (ΔV_{TH}) is defined as the difference between the threshold voltages ($\Delta V_{TH} = V_{TH}^{forward} - V_{TH}^{backward}$) in different sweep directions when the drain-source current is

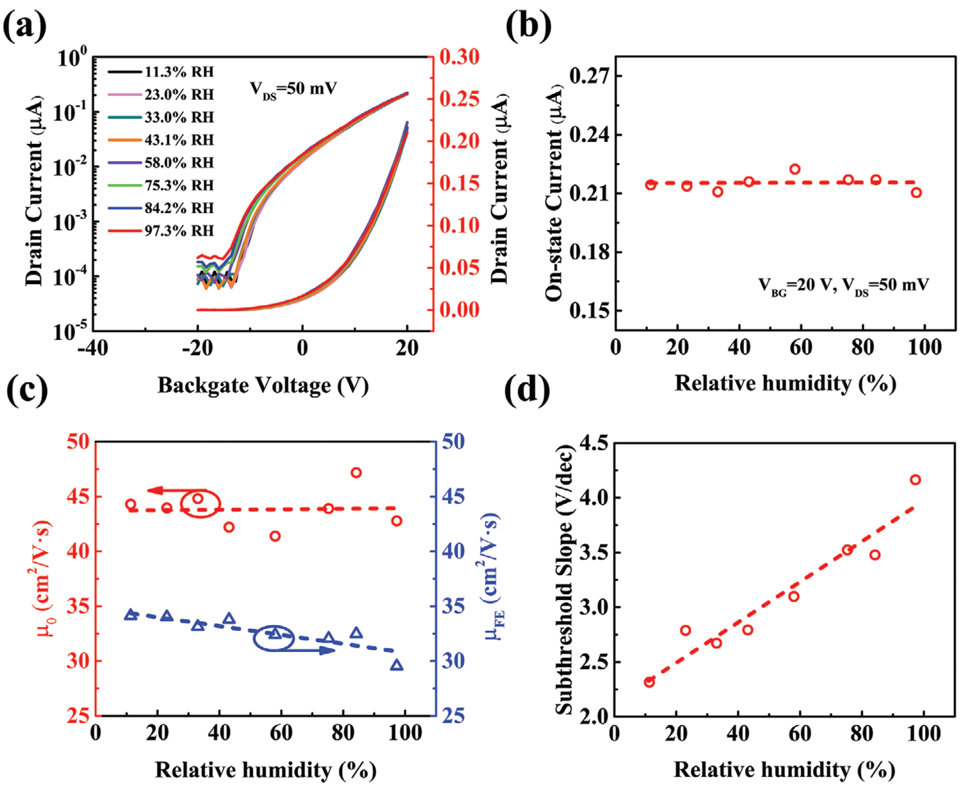

Figure 3. Electrical properties of the six-layer MoS_2 FET under different RHs. a) The transfer curves of the device with RHs increasing from 11.3% to 97.3% in both semi-logarithmic and linear scales ($V_{DS} = 50$ mV). b) The on-state current (I_{ON}) as functions of RH. c) The mobility, including the field-effect mobility (μ_{FE}) and the intrinsic mobility (μ_0), as functions of RH. d) The subthreshold slope (SS) as functions of RH.

1 nA. As shown in Figure 5b, the calculated hysteresis of tri-layer MoS_2 FET is in linear relationship with RH. Such a positive correlation indicates that the hysteresis is attributed to the adsorbed moisture at the top surface of MoS_2 film and that on top surface of SiO_2, where Si—OH silanol groups and water molecules are functioning.[42,43] The threshold voltages $V_{TH}^{forward}$ and $V_{TH}^{backward}$ under different RH are also shown in Figure 5b, which decrease significantly when RH increases. This result indicates that the water molecules serve as hole-trapping centers to effect the electrical properties of MoS_2 FET.[28] The detailed electrical characteristics including $V_{TH}^{forward}$, $V_{TH}^{backward}$, and ΔV_{TH} of the tri-layer MoS_2 FET are listed in Table S4, Supporting

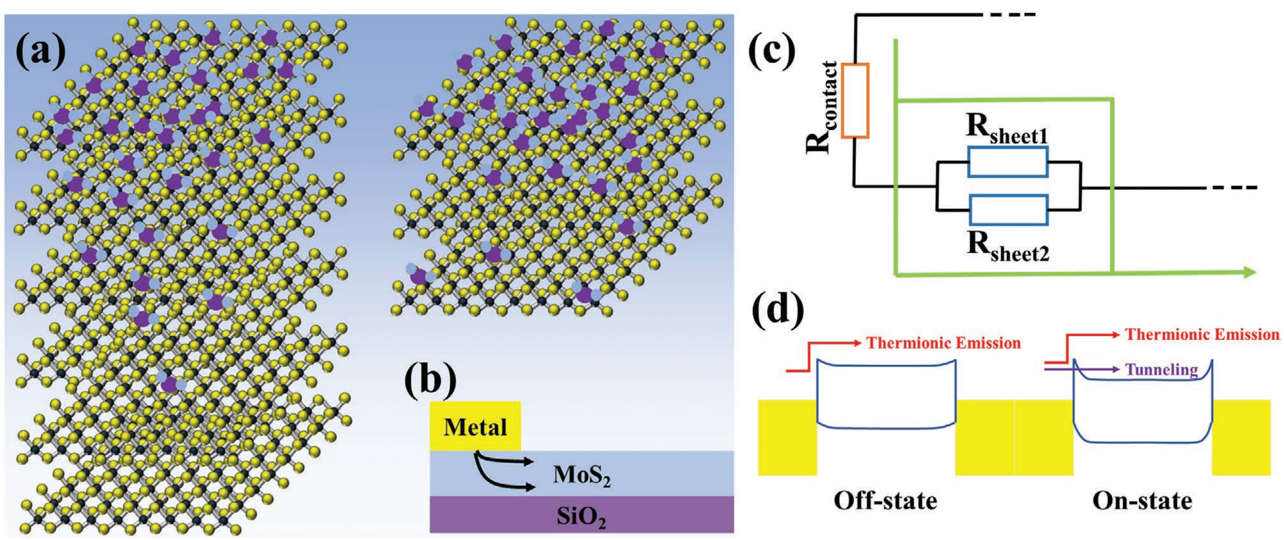

Figure 4. a) Schematic illustration of the permeation process of water molecules in the six-layer and tri-layer MoS_2 films. b) Schematic view of current flow across the metal/MoS_2. c) The resistor network model at the metal/semiconductor junction. d) Band diagrams of the few-layer MoS_2 FET.

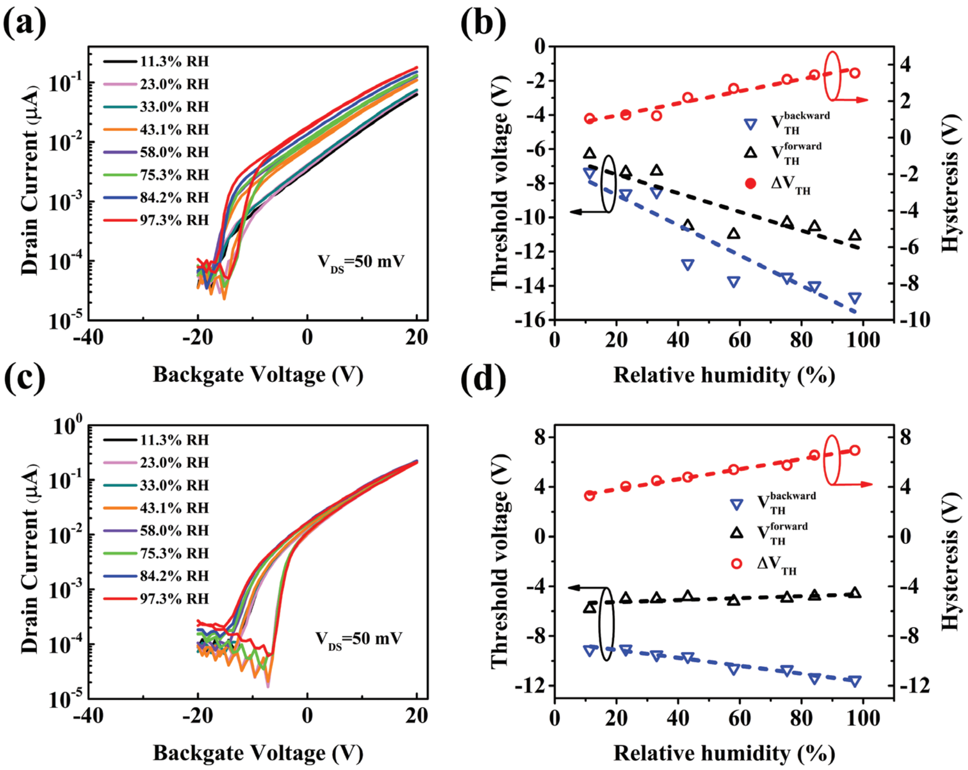

Figure 5. a) Double sweep transfer characteristics of the few-layer MoS_2 FET with RHs increasing from 11.3% to 97.3% in semi-logarithmic scale (V_{DS} = 50 mV). b) The backward threshold voltages (blue inverted triangle), forward threshold voltages (black regular triangle), and hysteresis (red circle) as functions of RH. c) Double sweep transfer characteristics of the six-layer MoS_2 FET with RHs increasing from 11.3% to 97.3% in semi-logarithmic scale (V_{DS} = 50 mV). d) The backward threshold voltages (blue inverted triangle), forward threshold voltages (black regular triangle), and hysteresis (red circle) as functions of RH.

Information. Similar to that of tri-layer MoS_2 FET, the transfer curves of the six-layer MoS_2 FET device show clockwise hysteresis characteristics related to RH, as shown in Figure 5c. The positive linear correlation between the hysteresis (ΔV_{TH}) and RH is also observed in six-layer MoS_2 FET as shown in Figure 5d. The threshold $V_{TH}^{forward}$ and $V_{TH}^{backward}$, which directly determined the value of ΔV_{TH}, are also plotted. When the RH increases, $V_{TH}^{backward}$ remains nearly constant while $V_{TH}^{forward}$ decreases significantly. Therefore, it is the variation in $V_{TH}^{forward}$ that results in the increased hysteresis, which indicates that water molecules dominantly act as hole-trapping centers. The variations of $V_{TH}^{forward}$, $V_{TH}^{backward}$, and ΔV_{TH} correspond well with the results of multilayer MoS_2 FET reported in ref. [28]. The detailed electrical characteristics including $V_{TH}^{forward}$, $V_{TH}^{backward}$, and ΔV_{TH} of the six-layer MoS_2 FET are listed in Table S5, Supporting Information. Furthermore, RH sensitivity of various normalized electrical parameters (I_{ON}, SS, μ_{FE}, μ_0, $V_{TH}^{forward}$, $V_{TH}^{backward}$, and ΔV_{TH}) are summarized in Figure S3, Supporting Information, which is helpful to understand few-layer MoS_2 as the active channel materials for humidity sensors.

3. Conclusion

In conclusion, the electrical properties of the back-gated tri- and six-layer MoS_2 FETs at different RHs (from 11.3% to 97.3%) were measured and discussed. The on-state current of tri-layer MoS_2 FET is more sensitive to RH than that of six-layer MoS_2 FET. A positive linear correlation between the hysteresis and RH is found in both tri- and six-layer MoS_2 FETs. We concluded that increasing the number of MoS_2 layers resulted in a less on-state current-RH dependence without significantly altering the hysteresis–RH dependence. The electrical properties of tri- and six-layer MoS_2 FETs under a wide range of RH studied in this work revealed the underlying mechanism of humidity sensing for few-layer MoS_2 thus paving the way for future humidity sensing application.

4. Experimental Section

Fabrication of MoS_2-Based FETs: MoS_2 flakes were mechanically exfoliated from bulk MoS_2 crystals (XFNANO Inc., Nanjing), and transferred onto a heavily doped p-type Si substrate with a 270 nm thick thermally grown SiO_2 film. Few-layer MoS_2 films were first identified by optical microscopy. Then MoS_2 films were characterized by Raman spectroscopy to determine the number of layers. An E-beam lithography was used for patterning the source and drain of the FETs, and Cr (5 nm)/Au (50 nm) were deposited by thermal evaporation to form the source and drain electrodes by the lift-off processing. To fabricate the MoS_2 FET for humidity sensing measurement, the substrate of few-layer MoS_2 FET was pasted into the Au pad of a carrying PCB, and the source/drain pads of MoS_2 FET were also bonded to the PCB.

Humidity Sensing Measurement: The humidity-dependent experiments were performed at an ambient temperature of ≈20 °C. The experimental setup used for studying the influence of humidity on the electrical characteristics of the few-layer MoS_2 FET devices is given in Figure S4, Supporting Information. Eight types of saturated salt solution were used to yield different RH levels. In order to minimize undesired light influence on the MoS_2 FET electrical performance, the experiments were carried out in darkness to prevent photogenerated carriers in MoS_2 semiconductor material. The humidity was increased in successive steps with a duration of 30 min each in order to obtain equilibrium state of the ambient as well as full absorption/desorption of water vapor. A commercial hygrometer (Rotronic HP22-A, ±0.8% RH) was placed inside the dark closed glass bottle for RH calibration. The electrical characteristics of device were measured using a semiconductor parameter analyzer (Tektronix, Keithley 4200-SCS).

Supporting Information

Supporting Information is available from the Wiley Online Library or from the author.

Acknowledgements

This work was supported by National Key Research and Development Program of China (Grant No. 2017YFA0204600), the National Natural Science Foundation of China (51872050, 61974034, and 61474028), Science and Technology Commission of Shanghai Municipality (Grant Nos. 19520744300, 18520744600, and 18520710800), and Ministry of Education Joint Fund for Equipment Pre-Research (No. 6141A02033241).

Conflict of Interest

The authors declare no conflict of interest.

Keywords

few-layer FETs, field effect transistors, humidity, hysteresis, molybdenum disulfide

Received: June 25, 2020
Revised: July 29, 2020
Published online: October 4, 2020

[1] S. Z. Butler, S. M. Hollen, L. Cao, Y. Cui, J. A. Gupta, H. R. Gutierrez, T. F. Heinz, S. S. Hong, J. X. Huang, A. F. Ismach, A. F. Ismach, *ACS Nano* **2013**, *7*, 2898.
[2] J. X. Chen, Z. L. Li, F. L. Ni, W. X. Ouyang, X. S. Fang, *Mater. Horiz.* **2020**, *7*, 1828.
[3] G. Fiori, F. Bonaccorso, G. Iannaccone, T. Palacios, D. Neumaier, A. Seabaugh, S. K. Banerjee, L. Colombo, *Nat. Nanotechnol.* **2014**, *9*, 768.
[4] S. Y. Li, Y. Zhang, W. Yang, H. Liu, X. S. Fang, *Adv. Mater.* **2020**, *32*, 1905443.
[5] W. Ouyang, J. X. Chen, J. H. He, X. S. Fang, *Adv. Electron. Mater.* **2020**, *6*, 2000168.
[6] S. X. Liu, L. X. Zheng, P. P. Yu, S. C. Han, X. S. Fang, *Adv. Funct. Mater.* **2016**, *26*, 3331.
[7] Z. J. Liu, C. H. Lin, B. R. Hyun, C. W. Sher, Z. J. Lv, B. Q. Luo, F. L. Jiang, T. Wu, C. H. Ho, H. C. Kuo, J. H. He, *Light Sci. Appl.* **2020**, *9*, 83.
[8] W. X. Ouyang, F. Teng, X. S. Fang, *Adv. Funct. Mater.* **2018**, *28*, 1707178.
[9] H. C. Fu, V. Ramalingam, H. Kim, C. H. Lin, X. S. Fang, H. N. Alshareef, J. H. He, *Adv. Energy Mater.* **2019**, *9*, 1900180.
[10] A. M. AlAmri, S. F. Leung, M. Vaseem, A. Shamim, J. H. He, *IEEE Trans. Elect. Dev.* **2019**, *66*, 2657.
[11] A. Alarawi, V. Ramalingam, H. C. Fu, P. Varadhan, R. S. Yang, J. H. He, *Opt. Express* **2019**, *27*, A352.
[12] H. Wang, L. L. Yu, Y. H. Lee, Y. M. Shi, A. Hsu, M. L. Chin, L. J. Li, M. Dubey, J. Kong, T. Palacios, *Nano Lett.* **2012**, *12*, 4674.
[13] Q. H. Wang, K. Kalantar-Zadeh, A. Kis, J. N. Coleman, M. S. Strano, *Nat. Nanotechnol.* **2012**, *7*, 699.
[14] Y. Yoon, K. Ganapathi, S. Salahuddin, *Nano Lett.* **2011**, *11*, 3768.
[15] L. X. Zheng, S. C. Han, H. Liu, P. P. Yu, X. S. Fang, *Small* **2016**, *12*, 1527.
[16] A. Nourbakhsh, A. Zubair, R. N. Sajjad, K. G. A. Tavakkoli, W. Chen, S. Fang, X. Ling, J. Kong, M. S. Dresselhaus, E. Kaxiras, K. K. Berggren, D. Antoniadis, T. Palacios, *Nano Lett.* **2016**, *16*, 7798.
[17] S. B. Desai, S. R. Madhvapathy, A. B. Sachid, J. P. Llinas, Q. X. Wang, G. H. Ahn, G. Pitner, M. J. Kim, J. Bokor, C. M. Hu, H. S. P. Wong, A. Javey, *Science* **2016**, *354*, 99.
[18] F. K. Perkins, A. L. Friedman, E. Cobas, P. M. Campbell, G. G. Jernigan, B. T. Jonker, *Nano Lett.* **2013**, *13*, 668.
[19] H. Qiu, L. J. Pan, Z. N. Yao, J. J. Li, Y. Shi, X. R. Wang, *Appl. Phys. Lett.* **2012**, *100*, 123104.
[20] H. J. Kwon, J. Jang, S. Kim, V. Subramanian, C. P. Grigoropoulos, *Appl. Phys. Lett.* **2014**, *105*, 152105.
[21] F. Ahmed, M. S. Choi, X. Liu, W. J. Yoo, *Nanoscale* **2015**, *7*, 9222.
[22] M. F. Khan, G. Nazir, V. M. Lermolenko, J. Eorn, *Sci. Technol. Adv. Mater.* **2016**, *17*, 166.
[23] D. J. Late, Y. K. Huang, B. Liu, J. Acharya, S. N. Shirodkar, J. J. Luo, A. M. Yan, D. Charles, U. V. Waghmare, V. P. Dravid, C. N. R. Rao, *ACS Nano* **2013**, *7*, 4879.
[24] J. P. Shu, G. T. Wu, S. Gao, B. Liu, X. L. Wei, Q. Chen, *Nanotechnology* **2017**, *28*, 204003.
[25] D. J. Late, B. Liu, H. S. S. R. Matte, V. P. Dravid, C. N. R. Rao, *ACS Nano* **2012**, *6*, 5635.
[26] J. Zhao, N. Li, H. Yu, Z. Wei, M. Z. Liao, P. Chen, S. P. Wang, D. X. Shi, Q. J. Sun, G. Y. Zhang, *Adv. Mater.* **2017**, *29*, 1702076.
[27] M. K. Chen, S. J. Wi, H. Nam, G. Priessnitz, X. G. Liang, *J. Vac. Sci. Technol. B* **2014**, *32*, 06FF02.
[28] Y. Shimazu, M. Tashiro, S. Sonobe, M. Takahashi, *Sci. Rep.* **2016**, *6*, 30084.
[29] C. Lee, H. Yan, L. E. Brus, T. F. Heinz, J. Hone, S. Ryu, *ACS Nano* **2010**, *4*, 2695.
[30] H. Li, Q. Zhang, C. C. R. Yap, B. K. Tay, T. H. T. Edwin, A. Olivier, D. Baillargeat, *Adv. Funct. Mater.* **2012**, *22*, 1385.
[31] K. L. Ganapathi, S. Bhattacharjee, S. Mohan, N. Bhat, *IEEE Electron Device Lett.* **2016**, *37*, 797.
[32] H. Yang, C. Li, L. Yue, C. Y. Wen, J. K. Zhang, D. P. Wu, *IEEE Electron Device Lett.* **2019**, *40*, 1116.
[33] M. A. Haque, A. Syed, F. H. Akhtar, R. Sheyate, S. Singh, K. V. Peinemann, D. Baran, T. Wu, *ACS Appl. Mater. Interfaces* **2019**, *11*, 29821.
[34] H. J. Kwon, J. Jang, S. Kim, V. Subramanian, C. P. Grigoropoulos, *Appl. Phys. Lett.* **2014**, *105*, 152105.
[35] J. M. Shin, J. H. Choi, D. H. Kim, H. K. Jang, J. Yun, J. Na, G. T. Kim, *Appl. Phys. Lett.* **2017**, *111*, 153105.
[36] P. Bolshakov, P. Zhao, A. Azcatl, P. K. Hurley, R. M. Wallace, C. D. Young, *Appl. Phys. Lett.* **2017**, *111*, 032110.
[37] R. Shevate, M. A. Haque, F. H. Akhtar, L. F. Villalobos, T. Wu, K. V. Peinemann, *Angew. Chem., Int. Ed.* **2018**, *57*, 11218.
[38] H. Liu, M. W. Si, Y. X. Deng, A. T. Neal, Y. C. Du, S. Najmaei, P. M. Ajayan, J. Lou, P. D. Ye, *ACS Nano* **2014**, *8*, 1031.
[39] Y. Y. Illarionov, G. Rzepa, M. Waltl, T. Knobloch, A. Grill, M. M. Furchi, T. Mueller, T. Grasser, *2D Mater.* **2016**, *3*, 035004.
[40] Q. A. Vu, S. Fan, S. H. Lee, M. K. Joo, W. J. Yu, Y. H. Lee, *2D Mater.* **2018**, *5*, 031001.
[41] A. Di Bartolomeo, L. Genovese, F. Giubileo, L. Iemmo, G. Luongo, T. Foller, M. Schleberger, *2D Mater.* **2018**, *5*, 015014.
[42] W. Kim, A. Javey, O. Vermesh, O. Wang, Y. M. Li, H. J. Dai, *Nano Lett.* **2003**, *3*, 193.
[43] A. Di Bartolomeo, M. Rinzan, A. K. Boyd, Y. F. Yang, L. Guadagno, F. Giubileo, P. Barbara, *Nanotechnology* **2010**, *21*, 115204.

